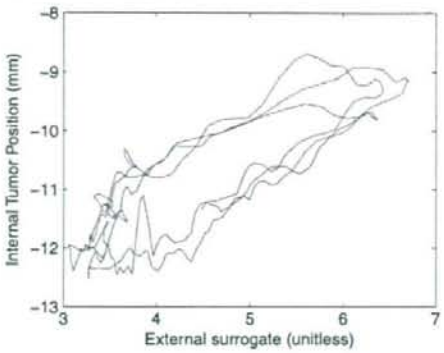

Figure 1. Example of a breathing trajectory with respiratory hysteresis.

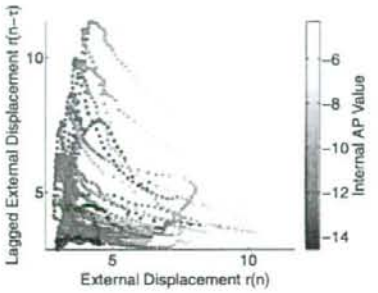

Figure 2. Scatter plot showing the data samples in augmented external state space with the colors indicating internal AP value. Locally consistent colored samples suggests the potential of resolving hysteretic ambiguity by distinguishing among different respiratory phases implicitly with state augmentation.

so direct inversion is numerically feasible. However, when more complicated models with higher degrees of freedom are used, it is desirable to reduce computation by applying recursive algorithms that modify current estimates based on newly available data. The key to recursively updating equation (5) is to avoid recomputing $(\boldsymbol{F}^T\boldsymbol{F})^{-1}$ from scratch every time. This is effectively the inversion of empirical correlation matrix with the observation $\boldsymbol{f}_t$. (Ruan *et al* 2008) provide rank-one update equations for sliding window and exponential discount adaptivities.

3. Results and discussions

To illustrate the challenges caused by hysteresis, figure 1 shows an example of the relationship between the internal tumor location obtained by fluoroscopic imaging and an external surrogate from an abdominal surface measurement as described in section 2.1. We depict only the anterior–posterior (AP) coordinate against the surrogate signal, as this axis demonstrates

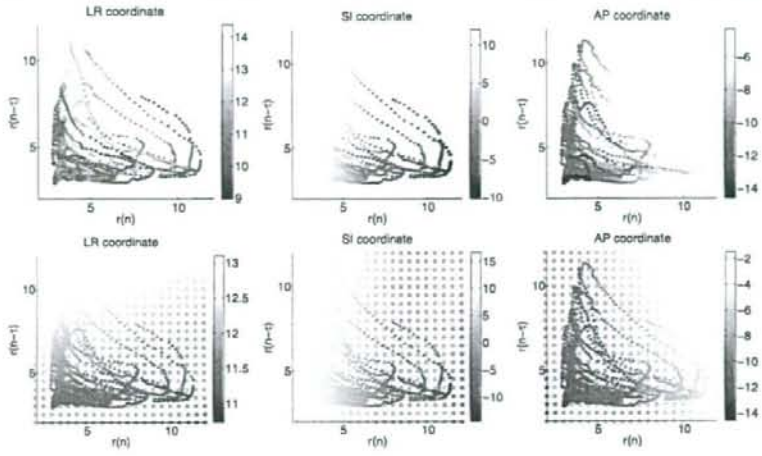

Figure 3. Correspondence relations in augmented state space and their linear fittings. Upper row: the internal tumor coordinate versus augmented state for observed samples with colors indicating internal AP value; bottom row: estimates of the tumor coordinate via linear fit with hollow circles depicting modeled hypersurface evaluated at regular grid points and solid circles for the evaluation at the sample locations, with colors indicating the estimated AP value.

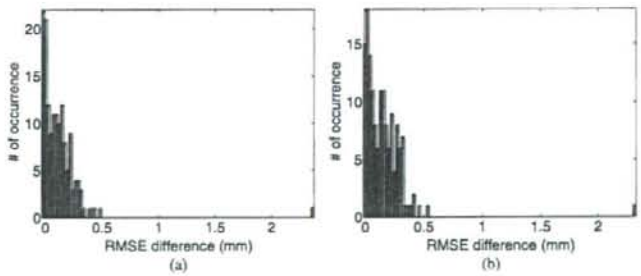

Figure 4. Histogram of paired differences between the RMS errors of the direct and augmented methods: (a) difference between the RMSE of the direct linear approach and augmented linear approach; (b) difference between the RMSE of the direct quadratic approach and augmented quadratic approach.

the strongest hysteresis for this test subject. The optimal linear and quadratic correspondence maps (Seppenwoolde *et al* 2007) provide a reasonable inference of the internal tumor motion from external surrogates, yet they fail to describe the breathing-phase dependency of an ideal correspondence map. In fact, any function that tries to map the scalar $r(n)$ to $\boldsymbol{p}$ would experience the same problem, since this is a one-to-multiple relation with hysteresis.

Figure 2 illustrates the internal tumor location in the anterior–posterior (AP) direction versus the state augmented external surrogates for $\tau = 45$, which corresponds to a 1.5 s delay

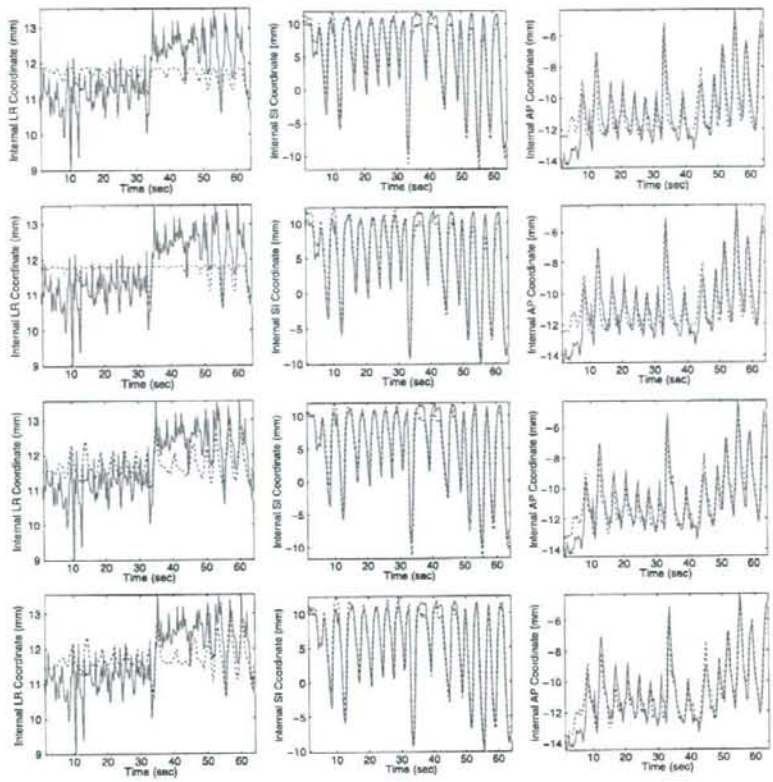

Figure 5. Estimation performance comparison among different methods. Red-solid line depicts the internal tumor position obtained from fluoroscopic imaging, and dashed-blue line provides estimated quantities from external surrogates. Each column represents one internal motion coordinate. Each row indicates the time series generated with one estimation method: (1st row) direct linear; (2nd row) direct polynomial; (3rd row) augmented linear; (bottom row) augmented polynomial.

for 30 Hz sampling rate. The scatter-plot in figure 2(a) represents each data sample in the $(r(n), r(n-\tau))$ space with a circle, and uses color (or intensity if viewed in the gray scale) to depict the internal AP coordinate values (in mm) from fluoroscopic readout. The one-to-multiple discrepancy appears largely resolved as different colored circles are not overlaid on each other, suggesting the existence of a single-valued inference map.

To illustrate the idea of model fitting in augmented state space, we first apply the simple linear model in equation (9) to the dataset shown in figure 1 with a lag length of 1.5 s (which may not be optimal), and illustrate the results in figure 3. Even though there are still noticeable differences between the observed internal coordinates in the upper row of figure 3 and their linear fit in the bottom row, the aggregated estimation error (across all patients and fractions)

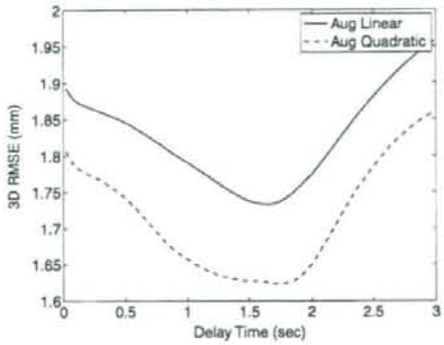

Figure 6. Estimation error as a function of lag length for state augmentation: linear fit (solid line); quadratic fit (dashed line).

reduced to 1.74 mm from 2.01 mm with direct linear fitting as in equation (2) and 1.93 mm with direct quadratic fitting as in equation (3). In particular, we observe noticeable decreases in estimation error in the AP direction, where hysteretic ambiguity is the most significant. Table 2 reports the root mean-squared error (RMSE) in each direction, respectively, for the linear and quadratic models, with and without state augmentation[6]. Figure 4 reports the paired (across patient/fraction) differences between the RMS error of the direct methods and the augmented methods. The RMSE difference between the direct linear and augmented linear methods has a mean of 0.14 mm and a median of 0.11 mm; the RMSE difference between the direct quadratic and augmented quadratic methods has a mean of 0.17 mm and a median of 0.15 mm. To assess statistical significance, we performed a paired Student's t-test with the null hypothesis that the performance of the direct and augmented methods do not differ. The p values for the linear method and the quadratic method are 4.96×10^{-13} and 4.08×10^{-18}, respectively, demonstrating that the error reductions were statistically significant.

Figure 5 shows the estimated time series of these four approaches for converting external surrogates to internal tumor locations. The higher-order models were more descriptive with the extra degrees of freedom, as demonstrated by the relative performance of quadratic models and linear models within each class respectively. State augmentation enables varying response patterns during different stages of breathing as indicated implicitly by the system dynamics.

As discussed in section 2.4, to properly choose the lag length , we use a short training set with internal–external pairs to compute offline the estimation performance $E(\hat{\boldsymbol{A}}(\tau))$ defined in equation (4) as a function of the lag length τ. In practice, the lag length does not have to be the exact optimum in equation (11); values near that optimum should sufficiently convey system dynamics. Reasonable insensitivity in the choice of lag length τ is desirable as this value is determined prior to the treatment and remains fixed subsequently. Figure 6 illustrates that the estimation error is a smooth function of the lag length, which suggests the desired robustness.

[6] For comparison purposes, we have also computed estimate from the fifth-order polynomial model with direct method, which has the same degrees of freedom (18 parameters) as the augmented quadratic model. Its estimation error is 0.75, 1.25 and 1.11 (mm) in LR, SI and AP direction respectively, with a 3D RMSE equals 1.83 mm. A paired Student's t-test between the RMSE for the fifth-order polynomial model and the augmented quadratic model yields a p-value of 1.06×10^{-10}, which indicates statistically significant error reduction by the augmented quadratic model. This shows that the improved performance of the proposed method is not a direct consequence of increased degrees of freedom, but should rather be attributed to its capability of resolving hysteretic ambiguity via state augmentation.

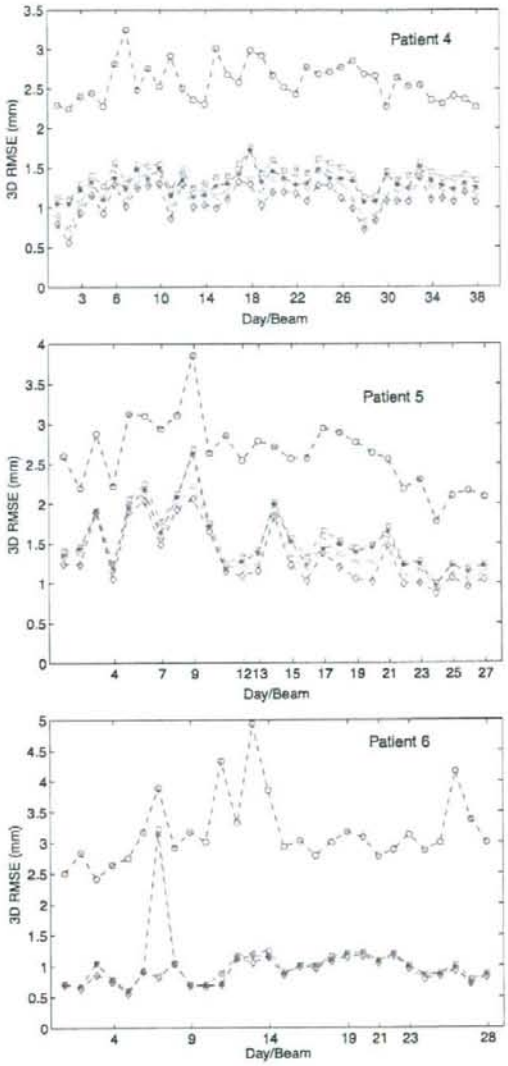

Figure 7. Beam-wise 3D RMSE (mm) for patients 4–6: minimum non-surrogate (blue circle-dashed); linear inference (green square-dashed); polynomial inference (red star-dashed); augmented linear inference (cyan triangle-dashed); augmented polynomial (magenta diamond-dashed). Non-uniform tick locations along the x-axis indicate the number of beams applied to each individual on the treatment day.

Table 2. Estimation error table.

	LR (mm)	SI (mm)	AP (mm)	3D (mm)
Direct linear	0.80	1.45	1.13	2.01
Direct quadratic	0.79	1.35	1.13	1.93
Aug. linear	0.75	1.30	0.87	1.74
Aug. quadratic	0.74	1.18	0.84	1.63

For both the linear correspondence model equation (9) and the second-order polynomial model equation (10) with state augmentation, the optimal τ corresponds to about 1.7–1.8 s delay. Without this knowledge, our previous experiments used 1.5 s delay to augment the state space (figures 2–5), and still yielded plausible results. The asymmetric slopes in figure (11) around the optimal $\hat{\tau}$ suggest that it may be preferable to use a relatively small time delay in the absence of precise information.

Assuming that the choice of lag length is robust to inter-patient and inter-fraction variations, we used a fixed lag length equivalent to 1.5 s delay for simplicity, and illustrate in figure 7 the beam-wise 3D RMSE for patients 4, 5 and 6, whose treatment extended over multiple days. The minimum RMS error for non-compensated treatment, which corresponds to a constant estimate at the retrospective mean value, is also shown for reference purposes. These results confirm that the augmented methods consistently exhibit lower error.

Adaptivity is most beneficial for irregular respiration traces. Our test data had relatively regular breathing patterns, so the inclusion of adaptivity improved the estimation accuracy only slightly.

4. Conclusion and future work

We have proposed a method to map external surrogate signals to internal tumor positions. Breathing-phase-dependent response patterns due to hysteresis are incorporated implicitly by using a simple state augmentation technique to capture system dynamics. We introduced a general class of correspondence models that are linear in model parameters, with the linear and quadratic (in external surrogate) models as special cases. We described closed-form expressions for both the optimal model parameters and the corresponding error value. Based on the latter, we further investigated the proper choice of lag length in state augmentation, and argued its relative robustness. Test results on clinical data demonstrated reduced inference error over the direct linear and polynomial models.

The number of degrees of freedom in a correspondence model determines the trade-off between flexibility and robustness. We seek a model that is descriptive enough to fit the data without undesired sensitivity to observation noise, also known as 'overfitting'. The proposed method may have more degrees of freedom than previous methods due to state augmentation. On the other hand, because it incorporates the breathing-stage information implicitly, it can use all the available internal–external correspondence pairs, without subdividing the training data as required for piecewise models (Seppenwoolde *et al* 2007, Lu *et al* 2005, Low *et al* 2005). In principle, using all the data may compensate for the possible increased sensitivity caused by the extra flexibility. The choice among different complexity levels in augmented models is still open. Both the number of augmentations and the model degree contribute to the overall complexity. Further studies should investigate methods for properly penalizing model complexity based on information criteria as explained in section 2.2.

Many research groups have observed phase shifts between external surrogate signals and internal tumor motions (Chi *et al* 2006, Ford *et al* 2003). Typically, this phase shift was to be

avoided to obtain higher internal–external correlation. However, it is possible to compensate for consistent phase shift, to simplify and improve the correspondence map estimation. In particular, we can artificially synchronize the internal–external phase by shifting one of them according to a constant offset estimated from training data. We will further study phase-offset estimation and its use in external–internal inference in the future.

This work is a preliminary study to validate the existence of a reasonably simple correspondence map and the possibility to estimate it with high accuracy. In practice, internal–external pairs are obtained at a much slower rate. Correspondence maps must be extracted from sparse imaging data and applied to continuously obtained external surrogate signals to estimate the internal tumor locations. Our method can serve as a critical module in this overall framework, yet intensive simulations and validations are further required.

Even though our test data did not exhibit dramatic improvements when using adaptive model estimation, model updates in response to changes are necessary in general. Pursuing this direction requires more thorough analysis of breathing motion variations, change detection and model adaptive rate.

Acknowledgments

We thank the reviewers for providing valuable insights and constructive suggestions in improving the quality of this work. This study is partially supported by the Barbour Fellowship at the University of Michigan and NIH grant P01-CA59827.

References

Ahn S, Yi B, Suh Y, Kim J, Lee S, Shin S, Shin S and Choi E 2004 A feasibility study on the prediction of tumor location in the lung from skin motion *Br. J. Radiol.* 77 588–96

Akaike H 1974 A new look at the statistical model identification *IEEE Trans. Autom. Control* 19 716–23

Berbeco R I, Nishioka S, Shirato H, Chen G T and Jiang S B 2005 Residual motion of lung tumors in gated radiotherapy with external respiratory surrogates *Phys. Med. Biol.* 50 3655–67

Chi P M, Balter P, Luo D, Mohan R and Pan T 2006 Relation of external surface to internal tumor motion studies with cine CT *Med. Phys.* 33 3116–23

Ford E C, Mageras G S, Yorke E and Ling C C 2003 Respiration-correlated spiral CT: a method of measuring respiratory-induced anatomic motion for radiation treatment planning *Med. Phys.* 30 88–97

Hoisak J D, Sixel K E, Tirona R, Cheung P C and Pignol J P 2004 Correlation of lung tumor motion with external surrogate indicators of respiration *Int. J. Radiat. Oncol. Biol. Phys.* 60 1298–306

Keall P J *et al* 2006 The management of respiratory motion in radiation oncology report of AAPM Task Group 76 *Med. Phys.* 33 3874–900

Koch N, Liu H H, Starkschall G, Jacobson M, Forster K, Liao Z, Komaki R and Stevens C W 2004 Evaluation of internal lung motion for respiratory-gated radiotherapy using MRI: part I. Correlating internal lung motion with skin fiducial motion *Int. J. Radiat. Oncol. Biol. Phys.* 60 1459–72

Kubo H D and Hill B C 1996 Respiration gated radiotherapy treatment: a technical study *Phys. Med. Biol.* 41 83–91

Low D A, Parikh P J, Lu W, Dempsey J F, Wahab S H, Hubenschmidt J P, Nystrom M M, Handoko M and Bradley J D 2005 Novel breathing motion model for radiotherapy *Int. J. Radiat. Oncol. Biol. Phys.* 63 921–9

Lu W *et al* 2005 Quantitation of the reconstruction quality of a four-dimensional computed tomography process for lung cancer patients *Med. Phys.* 32 890–901

Luenberger D G 1969 *Optimization by Vector Space Methods* (New York: Wiley)

Mageras G S *et al* 2004 Measurement of lung tumor motion using respiration-correlated CT *Int. J. Radiat. Oncol. Biol. Phys.* 60 933–41

Murphy M J 2004 Tracking moving organs in real time *Semin. Radiat. Oncol.* 14 91–100

Murphy M J, Jalden J and Isaksson M 2002 Adaptive filtering to predict lung tumor breathing motion during image-guided radiation therapy *Proc. 16th Int. Congr. on Computer-assisted Radiology and Surgery* pp 539–44

Ozhasoglu C and Murphy M J 2002 Issues in respiratory motion compensation during external-beam radiotherapy *Int. J. Radiat. Oncol. Biol. Phys.* 52 1389–99

Ruan D, Fessler J A and Balter J M 2008 Mean position tracking of respiratory motion *Med. Phys.* **35** 782–92
Schweikard A, Glosser G, Bodduluri M, Murphy M J and Adler J R 2000 Robotic motion compensation for respiratory movement during radiosurgery *Comput. Aided Surg.* **5** 263–77
Schweikard A, Shiomi H and Adler J 2004 Respiration tracking in radiosurgery *Med. Phys.* **31** 2738–41
Seppenwoolde Y, Berbeco R I, Nishioka S, Shirato H and Heijmen B 2007 Accuracy of tumor motion compensation algorithm from a robotic respiratory tracking system: a simulation study *Med. Phys.* **34** 2774–84
Seppenwoolde Y, Shirato H, Kitamura K, Shimizu S, van Herk M, Lebesque J V and Miyasaka K 2002 Precise and real-time measurement of 3D tumor motion in lung due to breathing and heartbeat, measured during radiotherapy *Int. J. Radiat. Oncol. Biol. Phys.* **53** 822–34
Shirato H *et al* 2000 Physical aspects of a real-time tumor-tracking system for gated radiotherapy *Int. J. Radiat. Oncol. Biol. Phys.* **48** 1187–95
Shirato H *et al* 2003 Feasibility of insertion/implantation of 2.0 mm diameter gold internal fiducial markers for precise setup and real-time tumor tracking in radiotherapy *Int. J. Radiat. Oncol. Biol. Phys.* **56** 240–7
Tsunashima Y, Sakae T, Shioyama Y, Kagei K, Terunuma T, Nohtomi A and Akine Y 2004 Correlation between the respiratory waveform measured using a respiratory sensor and 3D tumor motion in gated radiotherapy *Int. J. Radiat. Oncol. Biol. Phys.* **60** 951–8
Vedam S S, Kini V R, Keall P J, Ramakrishnan V, Mostafavi H and Mohan R 2003 Quantifying the predictability of diaphragm motion during respiration with a noninvasive external marker *Med. Phys.* **30** 505–13
Wade O L 1954 Movement of the thoracic cage and diaphragm in respiration *J. Physiol.* 193–212

IOP PUBLISHING PHYSICS IN MEDICINE AND BIOLOGY

Phys. Med. Biol. **53** (2008) 7137–7150 doi:10.1088/0031-9155/53/24/009

Gating based on internal/external signals with dynamic correlation updates

Huanmei Wu[1], Qingya Zhao[2], Ross I Berbeco[3], Seiko Nishioka[4], Hiroki Shirato[5] and Steve B Jiang[6]

[1] Purdue School of Engineering and Technology, Indiana University School of Informatics, IUPUI, Indianapolis, IN, USA
[2] School of Health Sciences, Purdue University, West Lafayette, IN, USA
[3] Department of Radiation Oncology, Dana-Farber/Brigham and Womens Cancer Center and Harvard Medical School, Boston, MA, USA
[4] NTT East-Japan Sapporo Hospital, Sapporo, Japan
[5] Hokkaido University Graduate School of Medicine, Sapporo, Japan
[6] Department of Radiation Oncology, School of Medicine, University of California, San Diego, CA, USA

E-mail: hw9@iupui.edu and sbjiang@ucsd.edu

Received 13 May 2008, in final form 27 October 2008
Published 26 November 2008
Online at stacks.iop.org/PMB/53/7137

Abstract

Precise localization of mobile tumor positions in real time is critical to the success of gated radiotherapy. Tumor positions are usually derived from either internal or external surrogates. Fluoroscopic gating based on internal surrogates, such as implanted fiducial markers, is accurate however requiring a large amount of imaging dose. Gating based on external surrogates, such as patient abdominal surface motion, is non-invasive however less accurate due to the uncertainty in the correlation between tumor location and external surrogates. To address these complications, we propose to investigate an approach based on hybrid gating with dynamic internal/external correlation updates. In this approach, the external signal is acquired at high frequency (such as 30 Hz) while the internal signal is sparsely acquired (such as 0.5 Hz or less). The internal signal is used to validate and update the internal/external correlation during treatment. Tumor positions are derived from the external signal based on the newly updated correlation. Two dynamic correlation updating algorithms are introduced. One is based on the motion amplitude and the other is based on the motion phase. Nine patients with synchronized internal/external motion signals are simulated retrospectively to evaluate the effectiveness of *hybrid gating*. The influences of different clinical conditions on hybrid gating, such as the size of gating windows, the optimal timing for internal signal acquisition and the acquisition frequency are investigated. The results demonstrate that dynamically updating the internal/external correlation in or around the gating window will reduce false positive with relatively diminished treatment efficiency. This improvement will benefit patients with

0031-9155/08/247137+14$30.00

mobile tumors, especially greater for early stage lung cancers, for which the tumors are less attached or freely floating in the lung.

(Some figures in this article are in colour only in the electronic version)

1. Introduction

It is well known that respiration-induced tumor motion will degrade the effectiveness of radiation treatment (Bortfeld *et al* 2002, Jiang *et al* 2003). Gated radiotherapy is an advanced radiation treatment method for tumors with respiratory motion (e.g., Jiang 2006) since gated treatment holds promise to reduce the incidence and severity of normal tissue complications and to increase local control through dose escalation (Keall *et al* 2002). However, due to the reduced clinical tumor volume to planning target volume (CTV-to-PTV) margin, the success of gated treatment largely depends upon precise target localization in real time.

Generally, gated treatments use various surrogates to derive tumor position during real-time treatment, although recent efforts have been made to generate gating signals from direct localization of the tumor mass (Berbeco *et al* 2005, Cui *et al* 2007). Gating based on internal surrogates (i.e., *internal gating*), such as the gold markers implanted in or near a tumor in the real-time tumor-tracking radiation therapy (RTRT) system (Shirato *et al* 2000a), has satisfactory precision. However, marker implantation is invasive and radiation dose to patients from fluoroscopic marker tracking is a big concern. With many treatment fractions or long treatment duration of a single fraction, the accumulative imaging dose can be more than is clinically acceptable (Jiang 2006). Gating based on external surrogates (i.e., *external gating*), such as markers placed on the surface of the patients' abdomen for the real-time position management (RPM) respiratory gating system (Kubo and Hill 1996, Vedam *et al* 2001) is easy, noninvasive, and radiation dose free. However, the precision is often less satisfactory (Berbeco *et al* 2005, Ionascu *et al* 2007, Seppenwoolde *et al* 2007).

Therefore, it is natural to combine the advantages of both internal and external gating. The goal is to reduce the internal imaging frequency by utilizing the external marker together with the internal marker. For effective gated treatment, updating the internal/external correlation in real time during treatment is required since it improves the confidences of external gating. One way of integrating internal/external markers has been explored on the CyberKnife System (Murphy 2004, Schweikard *et al* 2000). Markers on the patients' abdomen are constantly tracked and used to derive tumor positions. X-ray images are taken periodically (every 30 or 60 s) to re-calibrate the internal/external correlation. There is no correlation updating during a treatment beam. Kanoulas *et al* (2007) proposed an algorithm to update internal/external correlation with a fixed updating frequency (such as 10 Hz). Both methods acquire internal tumor positions at a fixed frequency and internal motion acquisition can occur at any stage of a breathing cycle. They are suitable for radiation treatment with beam tracking. However, they are not optimized for gated treatment.

We propose a *hybrid gating* technique which integrates the external and internal signals specially optimized for respiratory gating. This approach addresses some special concerns of gated treatment. For example, it ensures accurate internal/external correlation in or near the gating window although the correlation outside the gating window is not guaranteed. This paper will introduce two dynamic correlation updating algorithms optimized for hybrid gating with low-updating frequency ($\leqslant$0.2 Hz).

2. Methods and materials

2.1. Materials

We have retrospectively evaluated our proposed hybrid gating based on patient data collected at the Nippon Telegraph and Telephone Corporation (NTT) Hospital in Sapporo, Japan (Berbeco *et al* 2005). The 3D internal signals were acquired by fluoroscopic tracking of the implanted fiducial markers in or near the tumor with a Mitsubishi real-time tumor-tracking radiation therapy (RTRT) system (Shirato *et al* 2000a). The external signals are one-dimensional relative movement of patient abdominal surface, acquired through an external surrogate using the AZ-733V external respiratory gating system integrated with the RTRT system. The synchronized internal and external signals are gathered at 30 Hz throughout a treatment.

Nine lung patients with multiple ($\geqslant$4) treatment sessions are studied, of which the superior–inferior (SI) tumor motion is more than 7 mm. Only SI motion is studied in our hybrid gating since it is the most significant motion. Together, there are 154 treatment sessions for these nine patients. Detailed information about the patients studied has been introduced by other investigators (Berbeco *et al* 2005, Ionascu *et al* 2007).

2.2. Effects of correlation changes over gating treatment

Most patients exhibit one or more unsynchronized changes of amplitude variations, phase shifts and baseline drifts between internal and external motion signals. Examples are demonstrated in figure 1, which also shows the distinctive correlation patterns for the same patient at different times. The changes of internal/external correlation have great effects over gated treatment, which are illustrated in figure 2. The false positive is when the radiation beam is on while the tumor is out of the gating window. During a false positive, more radiation dose goes to healthy tissue and critical structures than was planned. The false negative is when the radiation beam is off while the tumor is in the gating window. From the point of clinical practice, a false positive is more serious than a false negative. Thus, the primary concern is to promote gating accuracy while maintaining an acceptable gating efficiency.

2.3. Gated treatment based on updated internal/external correlation

The proposed hybrid gating is a two-step procedure: *correlation initialization* (a pre-treatment step) and *correlation adjustment* (an online treatment step), which are introduced below:

(i) *Correlation initialization.* Before gated treatment, both the internal and external motion signals are acquired at high frequency (30 Hz for our test data) for a few breathing cycles. These high-frequency pre-treatment data will be applied to build the initial internal/external correlation. For the simulation presented in this paper, the training data are the first three full breathing cycles (a breathing cycle starts from the beginning of an exhale and ends at the end of the immediate next inhale). A variety of correlation algorithms can be used in this step. We have used the min max normalization (Han and Kamber 2006) in which the internal motion signal will not change while the external signal is scaled as follows:

$$e'(t) = \frac{(e(t) - e_{\min}) \cdot (x_{\max} - x_{\min})}{e_{\max} - e_{\min}} + x_{\min}, \tag{1}$$

where $e(t)$ and $e'(t)$ are the original and the correlated external signals, respectively, $e_{\max}$ and $e_{\min}$ (or $x_{\max}$ and $x_{\min}$) are the maximum and minimum values of the original external (or internal) signal.

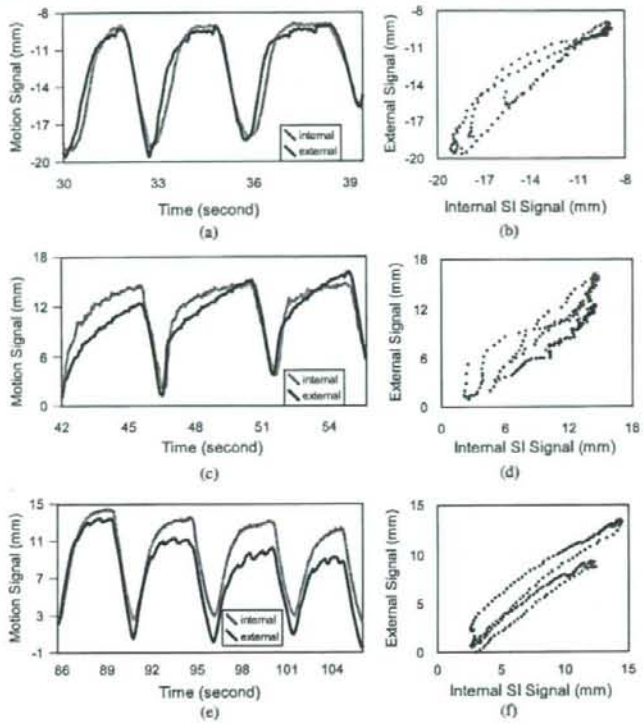

Figure 1. Internal/external motion signals and correlation patterns with phase shift (a) and (b), with baseline drift and amplitude variation (c) and (d) and with combination of phase shift, baseline drift and amplitude variation (e) and (f). The figures on the right (b), (d) and (f) display the internal/external correlations of the first (dark black dots) and last breathing cycles (gray dots) of each corresponding pair of motion signals.

(ii) *Correlation adjustment.* Due to changes of internal/external correlation over time, the initial correlation may not be a good reflection of the correlation during treatment. Updating the correlation in real time is necessary to accurately derive the internal tumor location based on the external signal. When an updating event occurs at t_i, the internal position is acquired, denoted as $x(t_i)$. Any external signal after t_i will be calculated according to the following equation:

$$e'(t) = e'_{\text{pre}}(t) - [e'_{\text{pre}}(t_i) - x(t_i)], \tag{2}$$

where $e'_{\text{pre}}(t)$ and $e'_{\text{pre}}(t_i)$ are the correlated external signals, at times t and t_i respectively, calculated based on the previous active correlation at t_i. Equation (2) will be the active correlation after t_i until the next updating event.

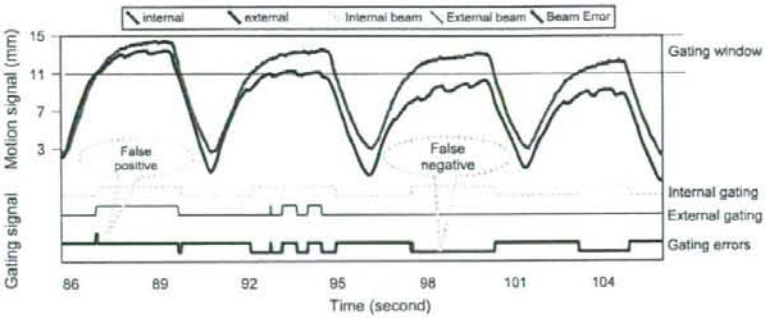

Figure 2. The effects of internal/external correlation changes over gated treatment. The internal gating shows the beam on and off based on internal motion signal while the external gating is based on the correlated external signal. Gating errors show the differences of internal and external gating.

It is critical to update the internal/external correlation when the tumor moves into the gating window to improve the effectiveness of gated treatment (supporting results are demonstrated in figure 6 and section 3.1). A successful updating algorithm needs to address two important issues: (*i*) *when* is the best time to update the correlation and (*ii*) *how* frequently an update is needed. This paper will describe two updating algorithms to determine the optimal updating time: one is based on the amplitude and the other is based on the phase.

- *Updating based on amplitude.* For this approach, the gating window is divided into different percentages based on amplitude, as illustrated in figure 3(a). One of these percentage lines is defined as the updating trigger line. Once the external signal passes the trigger line from below to above, an updating event will be triggered. Figure 3(a) demonstrates the corresponding updating events at the 0%, 25% and 50% percentage lines, for which the updating frequency is one update per breathing cycle. The amplitude-based updating is simple and straightforward. However, there can be no updating point for some breathing cycles. For instance, there is no update for the 50% percentage line for the first breathing cycle since the external signal never passes the 50% line in this breathing cycle. The worst case is that the external signal is always below the predefined amplitude percentage line. In this case, there will be no updates at all.
- *Update based on phase.* A piecewise linear representation (PLR) of respiratory motion (Wu *et al* 2004) decomposes a normal breathing cycle into three states: exhale (EX), end-of-exhale (EOE) and inhale (IN). The gating window (generally at the EOE state) for the external signal is divided into different phases based on the duration as demonstrated in figure 3(b). When the external signal passes the predefined triggering phase, the updating event will be activated. The phase-based algorithm ensures there is one updating point for every breathing cycle.

2.4. Gating window determination

We propose a clinical oriented approach to determining the gating window position, as shown in figure 4. The peak points at the EOE states are identified and the mean position of these peak

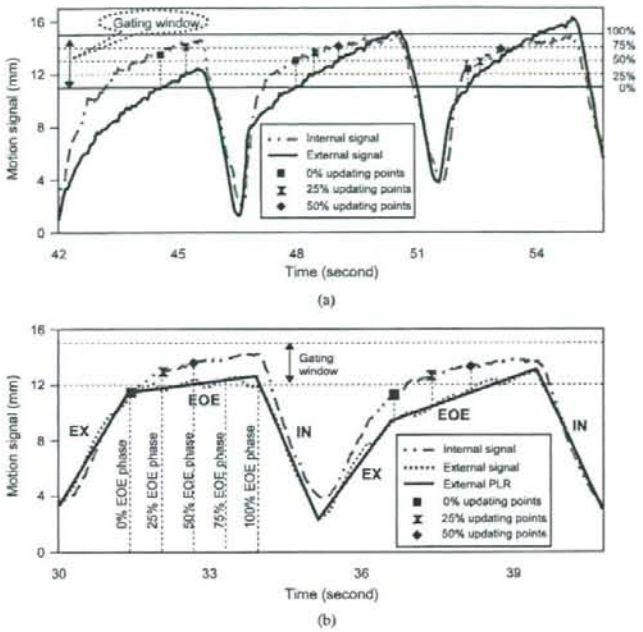

Figure 3. Two algorithms for online correlation adjustment during radiation treatment: (a) based on amplitude inside a gating window and (b) based on the phase of a piecewise linear model of external signal.

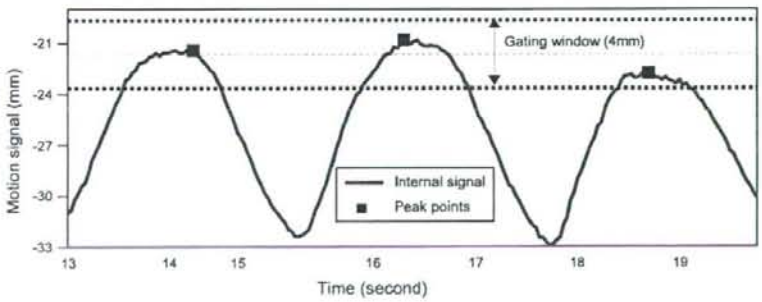

Figure 4. Determination of a gating window position based on the training data sets. The average of the peak points at the end-of-exhale is the center of the gating window.

points will be the middle position of the gating window. The simulation results presented in this paper use the first three breathing cycles to calculate the gating window position. Various

gating window sizes (from 2 mm to 6 mm) will then be simulated to assess the effect of gating window sizes on gated treatment.

2.5. Evaluation of hybrid gating

Three metrics, namely, *duty cycle*, *target coverage* and *residual motion*, are defined to retrospectively evaluate the outcomes of hybrid gating. Assuming t_0 is the total treatment duration, including both beam-on and beam-off time, t_1 is the beam-on time based on a specific updating algorithm (true positives plus false positives), and t_2 is the correct beam-on time (true positive), the two metrics are defined as follows:

$$\text{duty cycle (DC)} = \frac{t_1}{t_0} \cdot 100\%. \tag{3}$$

$$\text{target coverage (TC)} = \frac{t_2}{t_1} \cdot 100\%. \tag{4}$$

Both false positives and false negatives are considered in the two metrics. The more false negatives the lower the duty cycle. The more false positives the lower the target coverage. Ideally, a good hybrid gating algorithm should result in high DC and high TC. If a tradeoff between DC and TC is required, the focus is on improving TC while maintaining the DC at an acceptable level.

The residual motion is used to evaluate the statistical variability of the motion signals in the gating window. To calculate the residual motion, first, the motion position is classified either in or outside a gating window. The residual motion is the standard deviation of the corresponding motion signal inside the gating window, which is calculated based on the following formula:

$$\text{residual motion} = \sqrt{\left(x_i - \frac{\sum x_i}{n-1}\right)^2}, \tag{5}$$

where x_i is the motion signal inside a gating window of either the original signals or the updated signals.

The residual error between the internal target position and the edge of the gating window for all false positives is also measured. The relative average distance and total distance of false positives during a treatment fraction are calculated.

3. Results and discussion

The differences of hybrid gating with or without dynamic online adjustment of internal/external correlation are illustrated in figure 5. The updating algorithm is based on the piecewise linear model (PLR) at the 0% phase. It can be observed from the figure that both false positives and false negatives have been reduced for this specific patient. Similar results have been observed in the amplitude-based updating algorithm.

3.1. Results on the effects of updating timing

The optimal timing to update the internal/external correlation is an important issue for an updating algorithm. Figure 6 demonstrates the timing effects using amplitude-based updating algorithm. Nine timing options inside or outside the gating window at the exhale stage are illustrated in figure 6(a). The changes of target coverage (TC) and the duty cycle (DC) for one patient and the average for all the patients are illustrated in figures 6(b) and (c).

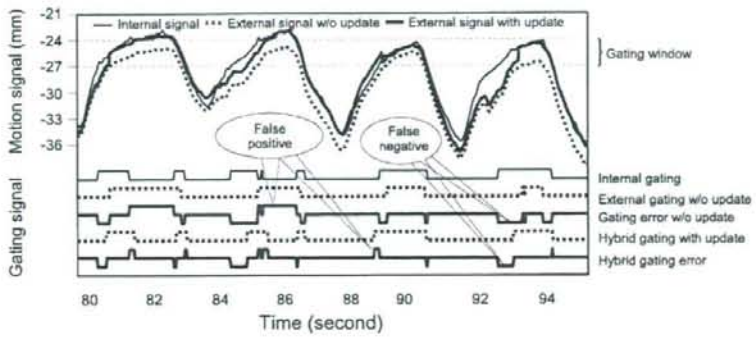

Figure 5. The outcome of hybrid gating with online adjustment of internal/external correlation based on the phase, along with the corresponding gating signals and gating errors.

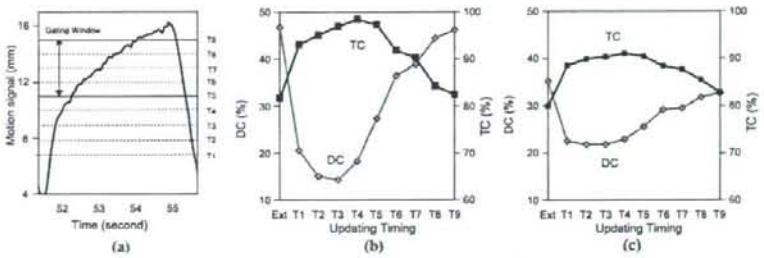

Figure 6. The timing effects on target coverage (TC) and duty cycle (DC) for amplitude-based updating where the updating frequency is once every cycle and the gating window size is 4 mm. (a) Illustration of the different updating points on the exhale state based on amplitude (b) the DC and TC changes for a specific patient averaged over 23 treatment sessions, and (c) the DC and TC changes averaged over 160 treatment sessions of nine patients.

The figures showed that hybrid gating with online correlation adjustment improves target coverage (TC), however it also brings down the duty cycle (DC). This is true at different timings. The improvement of TC is most prominent when the tumor moves into the gating window (updating timing T3, T4 and T5), i.e., near the transition points from exhale to end-of-exhale state. The improvement decreases as the updating timing is away from (both before or after) the transition points. The reduction of DC is significant in the exhale state but does not change too much in the end of exhale state.

The detailed effects of updating timings inside the gating window on gated treatments for nine patients are summarized in table 1. The phase-based updating yields similar results to the amplitude-based updating. A common observation from the table is that correlation updating will improve the target coverage but decrease the duty cycle inside the gating window. In addition, for most patients, updating at the earlier stage of the gating window shows greater improvements in the target coverage. In the following, we will focus on the updating results

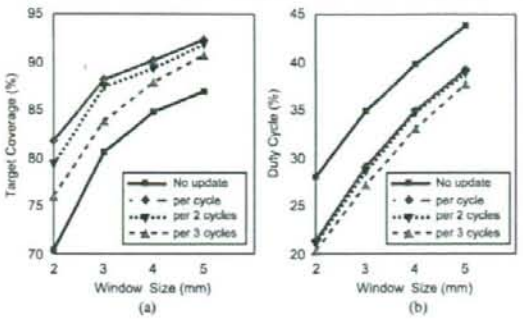

Figure 7. The effects of updating frequency on target coverage (TC) and duty cycle (DC) for amplitude-based updating, where the updating frequencies range from one update for every breathing cycle to one update for every three breathing cycles.

Table 1. The timing effects inside a gating window for amplitude-based updating of nine patients where gating window is 3 mm and updating frequency is once every cycle.

	TC (%)				DC (%)			
Patients	ext	T5	T6	T7	ext	T5	T6	T7
P1	75.39	90.46	90.02	85.40	21.39	20.42	19.59	16.28
P2	81.66	92.52	83.96	86.64	41.85	18.72	35.13	36.34
P3	78.93	94.48	90.86	89.78	40.77	20.07	29.71	30.86
P4	78.63	88.20	87.10	87.75	22.00	21.55	20.58	19.78
P5	77.53	96.52	93.00	90.47	33.19	21.28	22.89	22.58
P6	54.09	70.53	74.71	71.13	18.61	14.80	14.53	17.11
P7	55.76	75.00	82.18	77.32	40.36	11.02	17.35	19.83
P8	80.64	88.19	82.91	81.01	34.92	29.11	29.46	30.53
P9	77.56	84.36	87.66	85.59	19.93	23.11	21.79	19.89

on updating at lower edge of the gating window, i.e., the updating timing option T5 as shown in figure 6(a).

3.2. Results on the effects of updating frequencies

The choice of the updating frequency can be a challenging issue for real-time dynamic correlation updating. The effects of updating frequencies are demonstrated in figure 7 and table 2 for amplitude-based updating, where the updating frequencies range from one update per breathing cycle to one update every three breathing cycles. The average differences between updating every cycle and every two cycles are $1.65 \pm 0.26\%$ for TC (column $TC_1 - TC_2$) and $0.18 \pm 0.14\%$ for DC (column $DC_1 - DC_2$). The differences between updating every cycle and every three cycles are $4.98 \pm 1.34\%$ for TC and $0.63 \pm 0.55\%$ for DC. One notable exception is patient 9, who has extremely irregular external motion signal with erratic baseline shift, large amplitude oscillation, and frequency changes. Although its TC has improved with low-updating frequency, its DC has decreased. Similar results have been observed for the phase-based updating. The higher the frequency at which the updating

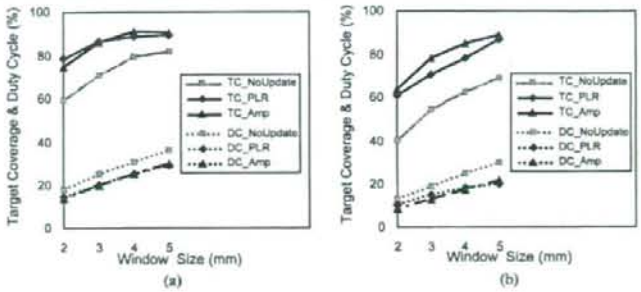

Figure 8. The effects of gating window sizes on target coverage (TC) and duty cycle (DC) for different external gating approaches (without updating, or updating based on amplitude or PLR): (a) for a patient with regular motion and (b) for a patient with erratic motion. The updating frequency is once per breathing cycle at 0% amplitude or EOE phase.

Table 2. The effects of the updating frequencies on amplitude-based updating where gating window size is 3 mm and the frequencies are one update per one (DC_1 and TC_1) or two (DC_2 and TC_2) or three (DC_3 and TC_3) breathing cycles.

	TC	(%)	DC	(%)
Patients	$TC_1 - TC_2$	$TC_1 - TC_3$	$DC_1 - DC_2$	$DC_1 - DC_3$
P1	2.62	14.36	−0.41	0.10
P2	0.60	4.45	0.17	−2.17
P3	1.03	4.78	−0.09	−3.25
P4	2.06	4.07	0.27	0.11
P5	1.60	3.97	0.23	−1.14
P6	1.92	3.43	−0.19	0.66
P7	2.57	0.43	0.94	−1.24
P8	0.79	4.35	0.55	1.92
P9	1.08	−9.51	0.46	−11.37
Average (P1 to P9)	1.65 ± 0.26	4.98 ± 1.34	0.18 ± 0.14	-0.63 ± 0.55

is performed, the better the target coverage (TC). The effects of updating frequencies are relatively small for DC.

3.3. Results on the effects of gating window sizes

The effects of gating window sizes on the efficacy of gated treatments have been analyzed and the results of two representative patients are illustrated in figure 8. Figure 8(a) shows a patient with regular motion and figure 8(b) shows one with quite irregular motion. The target coverage (TC) and duty cycle (DC) are compared among three gating approaches: external gating without correlation updating, hybrid gating with amplitude-based updating, and hybrid gating with phase-based updating. Generally, larger gating windows result in better target coverage and higher duty cycle. The duty cycle of most patients is $\geqslant 20\%$ when the gating window $\geqslant 3$mm.

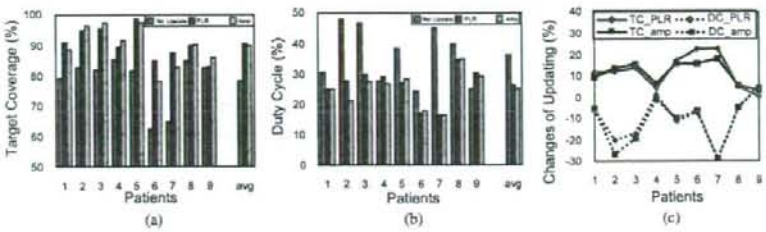

Figure 9. The results of dynamic correlations updating for gated treatments: (a) target coverage and (b) duty cycles and (c) changes of TC and DC induced by dynamic correlation updating. The 'avg' shows the TC and DC averaged over all patients.

The results show the impact of gating window size, which is restricted by the process of treatment planning. Most gated treatments use a gating window with fixed size and fixed position determined by the treatment planning process. Further investigation is needed to apply the proposed approach under clinical conditions, where the restriction of the treatment planning process will be taken into consideration.

3.4. Evaluation of dynamic updating on gated treatments

Figure 9 summarizes the target coverage (TC) and duty cycle (DC) for each patient, averaged over the whole treatment course. With dynamic updating, either amplitude- or phase-based updating, the target coverage is improved, notably for six patients (10% more than without updating), moderately for two patients, and slightly for one (patient 9 who has erratic motion). The average increase in TC, averaged over all patients, is 12% for phase-based updating and 11% for amplitude-based updating. However, the duty cycle has diminished with internal/external correlation updating (except patient 4 increases the DC by 1.3% for phase-based updating). The average decrease in DC is 10% for phase-based updating and 11% for amplitude-based updating.

Thus, applying either updating method will improve the outcome of gated treatment, although the phase-based approach showed slightly better performance than the amplitude-based approach for most patients. Target coverage demonstrates the precision of delivered radiation dose to the patients while the duty cycle indicates the duration of a gated treatment. Lower target coverage means more radiation dose to the healthy tissue or critical structures. From the view of clinical applications, as long as the duty cycle satisfies a certain threshold (such as at least 20%), the improvement of target coverage has great impact for precise radiation treatment.

3.5. Residual motion in the gating window

The residual motion, which is the standard deviation of the corresponding motion signal in the gating window, of two patients is illustrated in figure 10. One patient has regular motion and the other has irregular motion. It is shown that the residual motion has no significant difference whether the internal/external correlations are dynamically updated or not. Thus, our updating algorithms do not create large dispersion of the motion signals in the gating window.

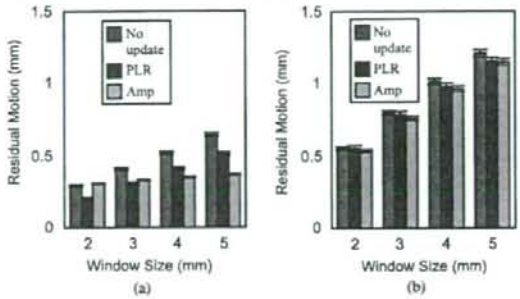

Figure 10. The residual motion in the gating window of the accumulative treatment signals: (a) the residual motion of a patient with regular motion and (b) the residual motion of a patient with irregular motion.

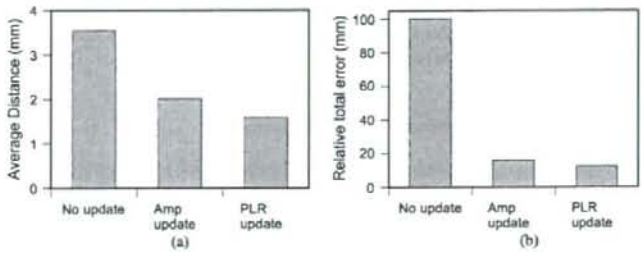

Figure 11. The false positive errors for a treatment session of a specific patient using different correlation approaches: (a) the average distance and (b) the total accumulative distances between the correlated tumor position and true internal position.

The errors between the internal target position and the edge of the gating window for all false positives are calculated. The average distances of a treatment fraction, either with or without update, are illustrated in figure 11(a), which showed that dynamic correlation updating reduced the residual error. The relative accumulative errors are demonstrated in figure 11(b), where the error without update is normalized to 100. For this treatment fraction, the relative accumulative errors with updates are less than 20 mm. One reason is that dynamic correlation updates reduce the false positive rate.

4. Summary

Two internal/external correlation updating algorithms have been proposed in this paper. One is based on the amplitude percentages in the gating window and the other is based on the phases of the end-of-exhale state (which usually is the gating window) from a piecewise linear representation (PLR) of motion signal. Comprehensive evaluation of gated treatment has been performed to test the effects of altered updating frequency, various gating window sizes, and